

Published in final edited form as:

Vision Res. 2009 August ; 49(17): 2157–2163. doi:10.1016/j.visres.2009.04.029.

A mathematical description of nerve fiber bundle trajectories and their variability in the human retina

N.M. Jansonius^{a,b,*}, J. Nevalainen^{c,1}, B. Selig^d, L.M. Zangwill^e, P.A. Sample^e, W.M. Budde^f, J.B. Jonas^g, W.A. Lagrèze^h, P.J. Airaksinen^c, R. Vontheinⁱ, L.A. Levin^{j,k}, J. Paetzold^d, and U. Schiefer^d

^a Department of Ophthalmology, University Medical Center Groningen, University of Groningen, Groningen, The Netherlands ^b Department of Epidemiology and Biostatistics, Erasmus Medical Center, Rotterdam, The Netherlands ^c University Eye Hospital Oulu, Finland ^d Centre for Ophthalmology, University of Tübingen, Germany ^e Hamilton Glaucoma Center, University of California, San Diego, USA ^f Private Practice, Essen-Steele, Germany ^g University Eye Hospital Mannheim, Germany ^h University Eye Hospital Freiburg, Germany ⁱ Department of Medical Biometry, University of Tübingen, Germany ^j Department of Ophthalmology and Visual Sciences, University of Wisconsin, Madison, USA ^k Department of Ophthalmology, University of Montreal, Canada

Abstract

We developed a mathematical model wherein retinal nerve fiber trajectories can be described and the corresponding inter-subject variability analyzed. The model was based on traced nerve fiber bundle trajectories extracted from 55 fundus photographs of 55 human subjects. The model resembled the typical retinal nerve fiber layer course within 20° eccentricity. Depending on the location of the visual field test point, the standard deviation of the calculated corresponding angular location at the optic nerve head circumference ranged from less than 1° to 18°, with an average of 8.8°.

Keywords

Glaucoma; Neuro-ophthalmology; Perimetry; Optic nerve head

1. Introduction

The loss of retinal nerve fiber bundles (RNFB) is a morphological sign of clinically manifest optic neuropathy. This has led to the use of standardized fundus photography of the retinal nerve fiber layer (RNFL) as a diagnostic tool, especially in glaucoma (Airaksinen & Alanko, 1983; Airaksinen, Drance, Douglas, Mawson, & Nieminen, 1984; Airaksinen, Drance, Douglas, Schulzer, & Wijsman, 1985; Airaksinen, Nieminen, & Mustonen, 1982; Iwata, Nanba, & Abe, 1982; Quigley et al., 1994; Sommer, D'Anna, Kues, & George, 1983). More recently, morphometric methods for analyzing and quantifying the optic nerve head (Heidelberg Retina Tomograph HRT; Heidelberg Engineering GmbH, Heidelberg, Germany; Rohrschneider, Burk, Kruse, & Völcker, 1994), the peri-papillary RNFL (nerve fiber analyzer GDx; Carl Zeiss Meditec Inc., Dublin, California, USA; Dreher & Reiter, 1992; Weinreb et

*Corresponding author. Address: Department of Ophthalmology, University Medical Center Groningen, University of Groningen, P.O. Box 30.001, 9700 RB Groningen, The Netherlands. Fax: +31 50 3611709. n.m.jansonius@ohk.umcg.nl, nomdo@dds.nl (N.M. Jansonius).

¹Contributed equally to this article.

al., 1990) or both (optical coherence tomograph OCT; Carl Zeiss Meditec AG, Jena, Germany; Hee et al., 1995) have been introduced.

A detailed knowledge of nerve fiber bundle trajectories is a prerequisite for a topographically precise prediction of circumscribed visual field loss from localized optic nerve head or peripapillary RNFL damage, and vice versa, which in turn is a prerequisite for new diagnostic techniques like fundus oriented perimetry (FOP; Schiefer et al., 2003) and scotoma oriented perimetry (SCOPE; Paetzold et al., 2005). Several attempts have been made to describe these nerve fiber bundle trajectories (Weber & Ulrich, 1991; Wigelius, 2001). A more detailed description of nerve fiber bundle trajectories was given by Garway-Heath, Poinoosawmy, Fitzke, and Hitchings (2000). They found a considerable variability and because of that variability they reported their findings as a schematic drawing showing a limited number of visual field sectors connected to 40° optic disc sectors. Obviously, this approach is not detailed enough to enable the new diagnostic techniques as listed above (FOP and SCOPE). Moreover, the drawing could erroneously be misinterpreted because of the sharp borders between the sectors.

The aim of the present study was to develop a robust mathematical framework wherein an elaborate description of the average course and variability of nerve fiber bundle trajectories can be given. For this purpose, nerve fiber bundle trajectories were extracted from fundus photographs and fitted by a mathematical model.

2. Methods

2.1. Patient data and data acquisition

All data were analyzed retrospectively and anonymously, according to the tenets of the Declaration of Helsinki. We collected digitized fundus images of 65 eyes of 65 subjects from the glaucoma services of five centers (University Eye Hospital Oulu, Finland; University Eye Hospital Mannheim, Germany; Hamilton Glaucoma Center, University of California, San Diego, USA; University Eye Hospital Freiburg, Germany; Centre for Ophthalmology, University of Tübingen, Germany). Fundus photographs of 10 eyes were excluded because the foveola could not be located precisely. One randomly chosen eye of each subject was included in the study. Thus, fundus images of 55 eyes of 55 subjects were analyzed. All visible RNFBs were electronically traced as far as visible by one of the authors (B.S.), resulting in 1660 RNFB trajectories traced with 16,816 sampling points. Only a limited number of these 1660 trajectories could be used because to be eligible for this study, trajectories had to have a minimum length and a minimum number of sampled data points and had to start within a certain distance from the center of the optic disk (see below).

Twenty seven of 55 fundus images were used to fit the nerve fiber trajectories by a mathematical model. The remaining 28 images were reserved as a test sample for an independent check of the model (validation procedure, see below).

2.2. Preprocessing

The position of the foveola and the center of the optic disc were marked on each image. The images were superimposed by translation in order to center the foveola, followed by rotation and zooming to align the centers of the optic discs (Fig. 1A), using graphic software (CorelDraw 10.0, Corel Inc., Ottawa, Canada). Tracings from left eyes were mirrored along the vertical axis to match tracings from right eyes.

2.3. Fitting fibers

The trajectories of the fibers were fitted in a modified polar coordinate system (r, φ) , with its center located in the center of the optic disc at an eccentricity of $15^\circ, 2^\circ$ above the horizontal meridian. Here, r represents the distance from the center of the disc and φ the corresponding angle, as illustrated in Fig. 1B. Details are given in Appendix A.

The basic assumption (see Section 4) was that a nerve fiber trajectory can be described in the above mentioned polar coordinate system (r, φ) by:

$$\varphi(\varphi_0, r) = \varphi_0 + b(\varphi_0) \cdot (r - r_0)^{c(\varphi_0)} \quad (1)$$

where $\varphi_0 = \varphi(r = r_0)$ is the angular position of the trajectory at its starting point at a circle with radius r_0 around the center of the disc, b a real number and c a positive real number. As mentioned above, to be eligible for this study, fiber recordings had to have a minimum length and a minimum number of sampled data points and had to start within a certain distance from the center of the optic disk. Table 1 summarizes these inclusion criteria as a function of φ_0 . As it was not possible to follow the fibers closer than typically $3\text{--}5^\circ$ to the center of the disk, r_0 was set to 4° . In this study, the analyses were limited to $180^\circ \geq \varphi_0 \geq 60^\circ$ (superior region) and $-60^\circ \geq \varphi_0 > -180^\circ$ (inferior region).

The fitting process consisted of three phases. First, all individual fibers were fitted by Eq. (1). In this fitting, c was quantized to $(0.5, 1.0, 1.5, \dots)$ and for each value of c , *RMS* values were calculated for each fiber according to:

$$RMS = \sqrt{\frac{1}{n} \sum_{i=1}^n (\varphi_i - \hat{\varphi}_i)^2} \quad (2)$$

where n is the number of sampled data points in the fiber, φ_i the measured value of φ for the i th data point and $\hat{\varphi}_i$ the corresponding fitted value. The c value yielding the lowest *RMS* value was recorded. Next, c was plotted as a function of φ_0 for all fibers together and the resulting relationship was substituted in Eq. (1). Finally, all fibers were fitted again to evaluate b as a function of φ_0 , including 95% limits (the range of b covering 95% of the included fibers). The variability of $\ln(b)$ was assumed to be independent of φ_0 and the 95% limits were calculated as plus or minus two times the standard deviation of the residuals, assuming normal distribution of the data. Normality was checked using a Shapiro–Francia W' test (Altman, 1991). All fits were performed with ASYST 3.10 (Asyst Software Technologies, Rochester, NY, USA), using the `curve.fit` and `gauss-newton.fit` routines.

2.4. Validation procedure

As an independent check, b values were determined for a test sample of fibers from a second, independent group of 28 fundus images, using c as a function of φ_0 as determined before. The resulting b values were compared to the 95% limits of b as found using the original sample.

2.5. Inverse model

An inverse of the model was evaluated numerically. For each point of the $30\text{--}26^\circ \times 6^\circ$ grid of the Humphrey field analyzer (Carl Zeiss Meditec Inc., Dublin, California, USA), the average value and the 95% limits of the corresponding angular location at the optic nerve head circumference were determined. These angular locations were transformed from our modified polar coordinate system to regular clock hours (with 0° corresponding to 3 o'clock in the right

eye, and so on), to enable an easier interpretation. For the inverse model, Mathematica 4.0.1.0 (Wolfram Research Inc., Champaign, IL, USA) was used.

3. Results

A mean of 30 RNFBs (range 3–118) could be traced in each image, with a mean of 10 sampling points per RNFB (range 3–48). Superimposition of the electronically traced fiber segments resembled the typical RNFL course within approximately 20° eccentricity (see Fig. 2A). One hundred and thirty three fibers fulfilled the strict criteria as stated in Table 1. The mean *RMS* was 0.87°, with a SD of 0.55° and a range from 0.10° to 2.70°. The median *RMS* was 0.69°. Fig. 2B shows a typical fit with an *RMS* value of 0.69°. Of these 133 fibers, 54 were located in the superior region ($180 \geq \varphi_0 \geq 60^\circ$) and 38 in the inferior region ($-60 \geq \varphi_0 > -180^\circ$). For the independent check, another 163 fibers fulfilled the criteria, of which 65 were located in the superior region and 58 in the inferior region.

Fig. 3 shows c as a function of φ_0 for the superior (A) and the inferior (B) region. As can be seen in this figure, c increases from the nasal side of the disk to the temporal side, from 0.5 to about 3 in the superior hemifield and from 0.5 to about 1.5 in the inferior hemifield. The continuous line in Fig. 3A is described by:

$$c=1.9+1.4\tanh\{-(\varphi_0 - 121)/14\} \quad (3)$$

and in Fig. 3B by:

$$c=1.0+0.5\tanh\{(-\varphi_0 - 90)/25\} \quad (4)$$

Fig. 4 presents b as a function of φ_0 for the superior (A) and the inferior (B) region. Fig. 5 shows the corresponding fits. Datapoints from both the original (diamond) and the independent (+) sample are shown. The continuous lines in Fig. 5A are described by:

$$\ln b = \beta_s + 3.9 \tanh\{ -(\varphi_0 - 121)/14 \} \quad (5)$$

where $\beta_s = -1.9$ for the mean value, -1.3 for the upper limit and -2.5 for the lower limit of $\ln b$. The residuals were normally distributed ($W' = 0.980$). The continuous lines in Fig. 5B are described by:

$$\ln(-b) = \beta_i + 1.5 \tanh\{ -(-\varphi_0 - 90)/25 \} \quad (6)$$

where $\beta_i = 0.7$ for the mean value, 1.3 for the upper limit and 0.1 for the lower limit of $\ln(-b)$. The residuals were normally distributed ($W' = 0.960$).

Fig. 6A presents the resulting model for the nerve fiber trajectories, in 10° steps. Fig. 6B gives the corresponding upper and lower limits, in 30° steps. Fig. 7 shows the reciprocal representation, with points from the 30–2 6° × 6° grid of the Humphrey Field Analyzer connected to the corresponding parts of the optic nerve head circumference. Depending on the location of the visual field test point, the standard deviation of this angular location at the optic nerve head circumference (calculated as one quarter of the 95% limits) ranged from less than 1° to 18°, with an average value of 8.8° (median 7.3°).

4. Discussion

This article presents a mathematical description of nerve fiber bundle trajectories in the human retina. The resulting model is robust as it relies on a limited number of free variables. Despite that, the model appeared to be flexible enough to describe a wide range of nerve fiber bundle trajectories as found in this study.

As mentioned in the Introduction, several descriptions of nerve fiber bundle trajectories have been given before. In his thesis, Wigelius (2001) gave a mathematical description that had an implicit solution similar to the course of the trajectories presented in this study. However, his aim, to fit the trajectory density on a circle around the optic disc and to estimate local RNFL thickness, was not achieved. Weber and Ulrich (1991) developed a RNFB map based on scotoma borders in RNFB defects. This map showed an about similar pattern as our model but was less complete and fine. Garway-Heath et al. (2000) estimated the correspondence of individual visual field test points (Humphrey Field Analyzer 24-2 $6 \times 6^\circ$ grid) and the circumference of the optic nerve head by tracing edges of RNFL defects from photographs of normal tension glaucoma patients. Our model appears to be in good agreement with their results. The variability at the level of the optic nerve head circumference they found, depicted by a standard deviation of 7.2° , appears to be surprisingly similar to our mean value of 8.8° (median 7.3°). We showed that this standard deviation depends largely on the location of the visual field test point (from less than 1° to 18°). Hoffmann, Medeiros, Sample, Boden, Bowd, et al. (2006) studied the association between patterns of visual field loss and RNFL thickness measurements using scanning laser polarimetry. Visual field defects in the superior hemifield were associated with RNFL defects in the inferior hemiretina, and *vice versa*, but a detailed topographic association could not be found.

Although the variability found in this study was in good agreement with earlier findings (see above), sources of variability other than real variability in the wiring of the human retina have to be considered. One possible source of variability is the choice of our basic equation used to describe individual nerve fiber trajectories, Eq. (1). We started our modeling with Taylor polynomials. It turned out that most fibers could be easily be described with just a single term of such a polynomial, but different powers were needed in different regions. That resulted in the use of Eq. (1). The quality of this approach was quantified with an RMS value, and a fit of a trajectory with a median RMS value was presented in Fig. 2B. Obviously, the variability found in this study was not related to the choice of our basic equation. Another source of variability might be the evaluation process of the parameters b and c . As this evaluation process required non-linear fitting, parameters b and c were evaluated in a two-stage process. To check this process, the final results were checked graphically by drawing, for a large number of fibers, individual measured trajectories and the calculated limits wherein they should be, given their clock hour at the disk margin. The vast majority of the trajectories indeed run within the limits, without giving the impression that the limits were too wide. Hence, the variability must reflect real variability in the wiring of the human retina.

The model as presented in this study was built in a novel coordinate system, described in the Methods and Appendix A Sections. The choice of a coordinate system is essentially arbitrary as long as proper transformations are performed going from one system to the other (Boyer, 1949). Usually, a system is chosen that makes the mathematics as simple as possible. In nerve fiber trajectory analysis, the horizontal raphe and the center of the optic disc are the natural anatomical beacons. Since the horizontal raphe is not entirely straight (but slightly bended between fovea and disc), it cannot serve as a classical cartesian x -axis. Likewise, the disc cannot serve as the center of a classical polar coordinate system, because the disc is located slightly above the x -axis as defined by the straight part of the horizontal raphe. The modified polar coordinate system as used in this study fits in the anatomy of the retina, having the disc in the

center and the horizontal raphe defined by a single φ value. Our modified polar coordinate system belongs to the general family of “curvilinear coordinate systems”; it fulfills all requirements of a curvilinear system: same number of coordinates, one-to-one projections (bijections) and smooth functions. It should be stressed that the transformations do not distort the image; distortions only occur when dimensions are reduced, like plotting earth [3D] on a map [2D].

This analysis was based on a heterogeneous set of fundus images. Photographs were collected from anonymized databases and biometric data were not available. This lack of biometric data precluded the determination of the influence of axial length from this dataset. We will address the influence of axial length in a future study. It is known that age, media opacities and myopia are inversely correlated with visibility of the RNFL (Bowd, Weinreb, Williams, & Zangwill, 2000; Jonas & Dichtl, 1996; Jonas & Schiro, 1993; Serguhn & Gramer, 1997; Tanito, Itai, Ohira, & Chihara, 2004; Tuulonen et al., 2000). As a result, the fibers included in this study may form a biased sample. We had the option to exclude fundi with only a limited number of visible trajectories completely, but that would have increased rather than decreased the inevitable selection bias.

Visibility of the RNFBs and of RNFL defects is best in the peripapillary region and deteriorates towards the periphery (Jonas, Nguyen, & Naumann, 1989; Jonas & Schiro, 1993). Moreover, fundus photographs only reveal a two-dimensional impression of the RNFL, which is in reality arranged in a three-dimensional pattern: the most superficial RNFB layers (adjacent to the vitreous body) represent the central region; the deeper layers originate from the retinal periphery (Airaksinen & Alanko, 1983; Minckler, 1980). As a consequence of this arrangement, fibers from the periphery – even if visible in the periphery – cannot be traced back to the optic disk. For these reasons, the analyses were limited to 20° eccentricity.

Measured trajectories were virtually absent in the papillomacular bundle ($160^\circ < |\varphi_0| \leq 180^\circ$). The extrapolation as presented here obviously depends on the model and may actually reflect a rather poor description of the papillomacular bundle. Likewise, too little information was available from the nasal region and therefore we limited the current model to $|\varphi_0| \geq 60^\circ$. If the model would be applied to glaucoma, these would be no real limitations since the papillomacular bundle and the nasal retina are rarely affected in all but the end stage of this disease.

In summary, this study confirms the presence of considerable variability of the nerve fiber bundle trajectories in the human retina, yields a detailed location-specific estimate of the magnitude of this variability, and provides a useful mathematical tool for further analyzing it.

References

- Airaksinen PJ, Alanko HI. Effect of retinal nerve fibre loss on the optic nerve head configuration in early glaucoma. *Graefes Archive of Clinical and Experimental Ophthalmology* 1983;220:193–196.
- Airaksinen PJ, Drance SM, Douglas GR, Mawson DK, Nieminen H. Diffuse and localized nerve fiber loss in glaucoma. *American Journal of Ophthalmology* 1984;98:566–571. [PubMed: 6496612]
- Airaksinen PJ, Drance SM, Douglas GR, Schulzer M, Wijsman K. Visual field and retinal nerve fiber layer comparisons in glaucoma. *Archives of Ophthalmology* 1985;103:205–207. [PubMed: 3977691]
- Airaksinen PJ, Nieminen J, Mustonen HE. Retinal nerve fiber layer photography with a wide angle fundus camera. *Acta Ophthalmologica (Copenhagen)* 1982;60:362–368.
- Altman, DG. *Practical statistics for medical research*. London: Chapman & Hall; 1991.
- Bowd C, Weinreb RN, Williams JM, Zangwill LM. The retinal nerve fiber layer thickness in ocular hypertensive, normal, and glaucomatous eyes with optical coherence tomography. *Archives of Ophthalmology* 2000;118:22–26. [PubMed: 10636409]

- Boyer CB. Newton as an originator of polar coordinates. *The American Mathematical Monthly* 1949;56:73–78.
- Dreher AW, Reiter K. Retinal laser ellipsometry – A new method for measuring the retinal nerve fiber layer thickness distribution. *Clinical Vision Science* 1992;7:481–488.
- Garway-Heath DF, Poinoosawmy D, Fitzke FW, Hitchings RA. Mapping the visual field to the optic disc in normal tension glaucoma eyes. *Ophthalmology* 2000;107:1809–1815. [PubMed: 11013178]
- Hee MR, Izatt JA, Swanson EA, Huang D, Schuman JS, Lin CP, et al. Optical coherence tomography of the human retina. *Archives of Ophthalmology* 1995;113:325–332. [PubMed: 7887846]
- Hoffmann EM, Medeiros FA, Sample PA, Boden C, Bowd C, Bourne RR, et al. Relationship between patterns of visual field loss and retinal nerve fiber layer thickness measurements. *American Journal of Ophthalmology* 2006;141:463–471. [PubMed: 16490491]
- Iwata K, Nanba K, Abe H. Die beginnende Fundusveränderung infolge rezidivierender kleiner Krisen beim Posner-Schlossman-Syndrom – ein Modell für das Glaucoma simplex. *Klinisch Monatsblatt der Augenheilkunde* 1982;180:20–26.
- Jonas JB, Dichtl A. Evaluation of the retinal nerve fiber layer. *Survey of Ophthalmology* 1996;40:369–378. [PubMed: 8779083]
- Jonas JB, Nguyen NX, Naumann GOH. The retinal nerve fiber layer in normal eyes. *Ophthalmology* 1989;96:627–632. [PubMed: 2748120]
- Jonas JB, Schiro D. Visibility of the normal retinal nerve fiber layer correlated with rim width and vessel caliber. *Graefe's Archive of Clinical and Experimental Ophthalmology* 1993;231:207–211.
- Minckler DS. The organization of nerve fiber bundles in the primate optic nerve head. *Archives of Ophthalmology* 1980;98:1630–1636. [PubMed: 6158937]
- Paetzold J, Sample PA, Selig B, Krapp E, Vonthein R, Schiefer U. Differentiation between glaucomatous scotoma progression in depth and in size by using scotoma-oriented perimetry (SCOPE) with locally condensed stimulus arrangements. *Investigative Ophthalmology and Vision Science* 2005;46 (E-Abstract 636).
- Quigley HA, Enger C, Katz J, Sommer A, Scott R, Gilbert D. Risk factors for the development of glaucomatous visual field loss in ocular hypertension. *Archives of Ophthalmology* 1994;112:644–649. [PubMed: 8185522]
- Rohrschneider K, Burk RO, Kruse FE, Völcker HE. Reproducibility of the optic nerve head topography with a new laser tomographic scanning device. *Ophthalmology* 1994;101:1044–1049. [PubMed: 8008345]
- Schiefer U, Flad M, Stumpp F, Malsam A, Paetzold J, Vonthein R, et al. Increased detection rate of glaucomatous visual field damage with locally condensed grids: a comparison between fundus-oriented perimetry and conventional visual field examination. *Archives of Ophthalmology* 2003;121:458–465. [PubMed: 12695242]
- Serguhn, S.; Gramer, E. *Perimetry Update 1996/1997*. Amsterdam: Kugler; 1997. Nerve fiber layer thickness evaluation in the upper and lower retinal half using the nerve fiber analyzer in a clinical study; p. 163-171.
- Sommer A, D'Anna SA, Kues HA, George T. High-resolution photography of the retinal nerve fiber layer. *American Journal of Ophthalmology* 1983;96:535–539. [PubMed: 6624835]
- Tanito M, Itai N, Ohira A, Chihara E. Reduction of posterior pole retinal thickness in glaucoma detected using the retinal thickness analyzer. *Ophthalmology* 2004;111:265–275. [PubMed: 15019374]
- Tuulonen A, Alanko H, Hyytinen P, Veijola J, Seppanen T, Airaksinen PJ. Digital imaging and microtexture analysis of the nerve fiber layer. *Journal of Glaucoma* 2000;9:5–9. [PubMed: 10708225]
- Weber J, Ulrich H. A perimetric nerve fiber bundle map. *International Ophthalmology* 1991;15:193–200. [PubMed: 2050474]
- Weinreb RN, Dreher AW, Coleman A, Quigley H, Shaw B, Reiter K. Histopathologic validation of Fourier-ellipsometry measurements of retinal nerve fiber layer thickness. *Archives of Ophthalmology* 1990;108:557–560. [PubMed: 2322159]
- Wigelius, O. Master's thesis in mathematical sciences. Lund University; Sweden: 2001. A model for the retinal nerve fiber layer.

Appendix A

The trajectories of the RNFBs were described in a modified polar coordinate system (r, φ) with its center located in the center of the optic disc (Fig. 1B). The transformation from the cartesian coordinate system with its center at the fovea (x, y) to this polar coordinate system is done in two steps. First, transformation to a modified cartesian coordinate system with its center located at the center of the optic disk (x', y') :

$$x' = x - 15 \quad (7)$$

$$y' = y - 2(x/15)^2 \text{ for } x > 0 \quad (8a)$$

$$y' = y \text{ else} \quad (8b)$$

Second, transformation to polar coordinates (r, φ) :

$$r = \text{sqrt} \left[(x')^2 + (y')^2 \right] \quad (9)$$

$$\varphi = \text{arctan}(y' / x') \quad (10)$$

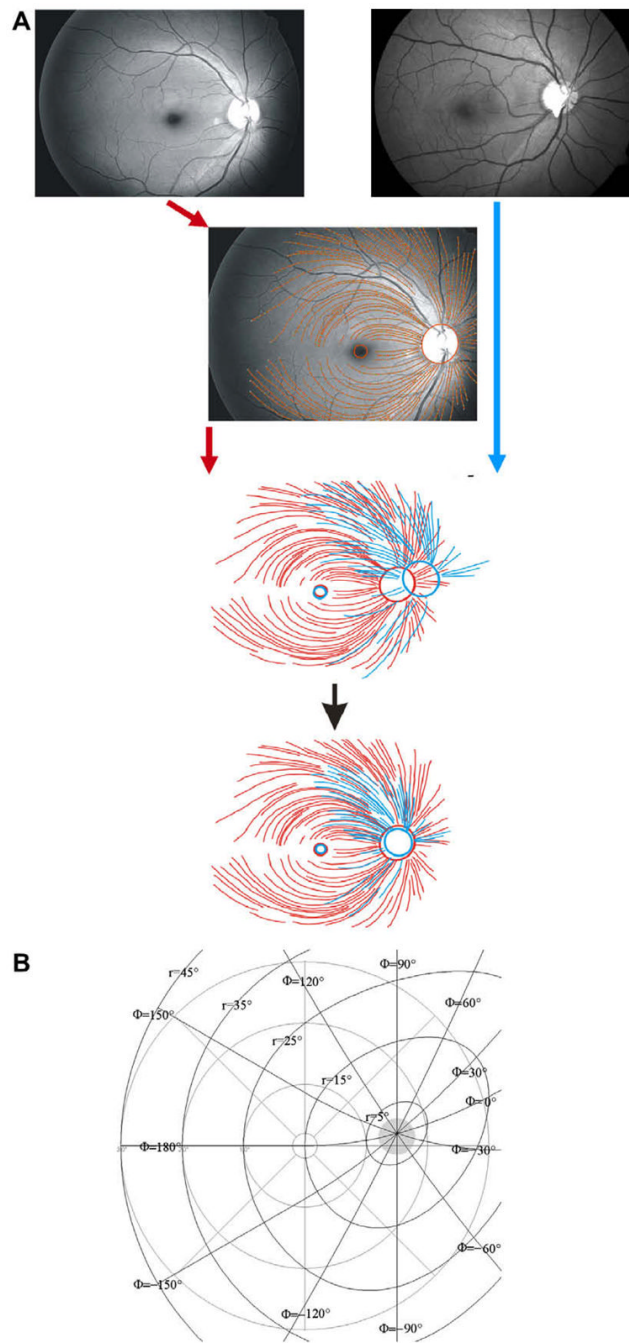


Fig. 1. Illustration of the superimposition process. First, images are translated in order to center the foveolae. Next, the images are zoomed and rotated in order to center the optic disks (A). Illustration of the modified polar coordinate system (B); for details see Appendix A.

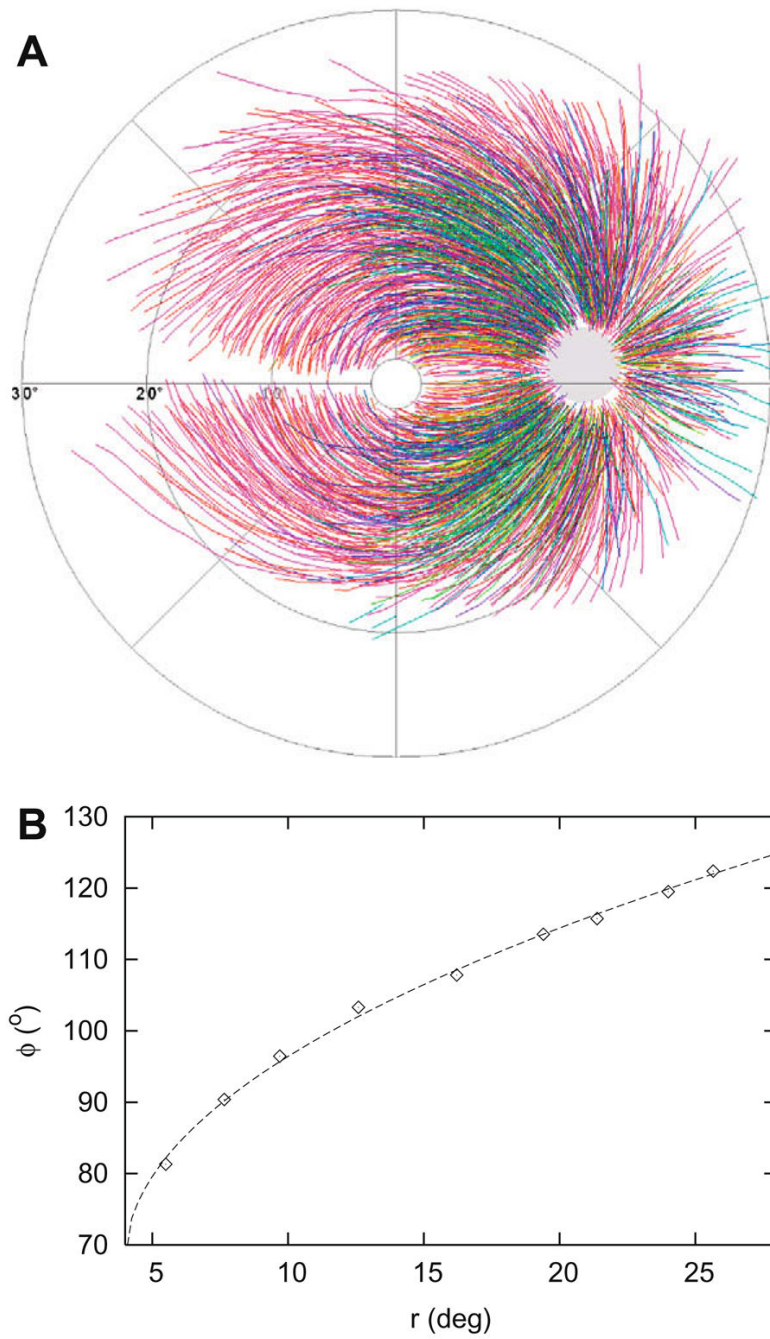


Fig. 2. Superimposition of all 1660 sampled fibers (A). Example of a fit by Eq. (1) of a single fiber with $c = 0.5$, $\varphi_0 = 68^\circ$, $n = 9$ and $RMS = 0.69$ (B).

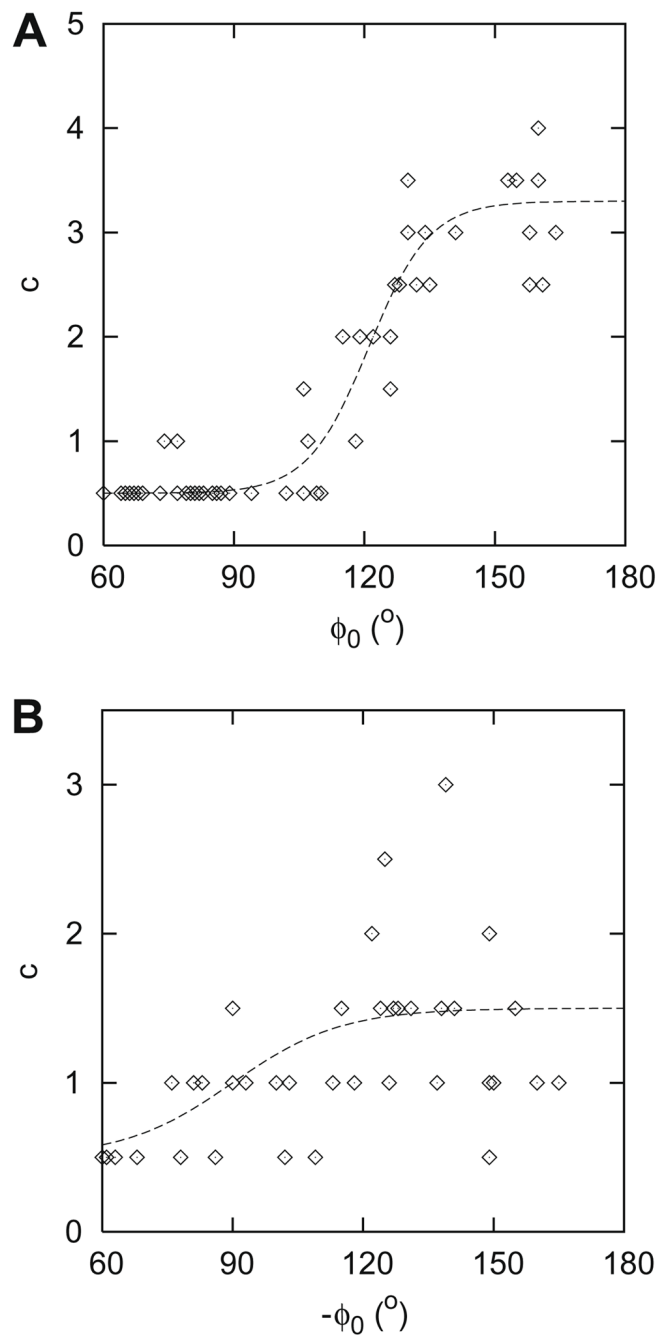


Fig. 3. Parameter c (as defined in Eq. (1)) as a function of ϕ_0 for the superior (A) and the inferior (B) hemifield. The continuous lines represent the corresponding fits as described in Eqs. (3) and (4).

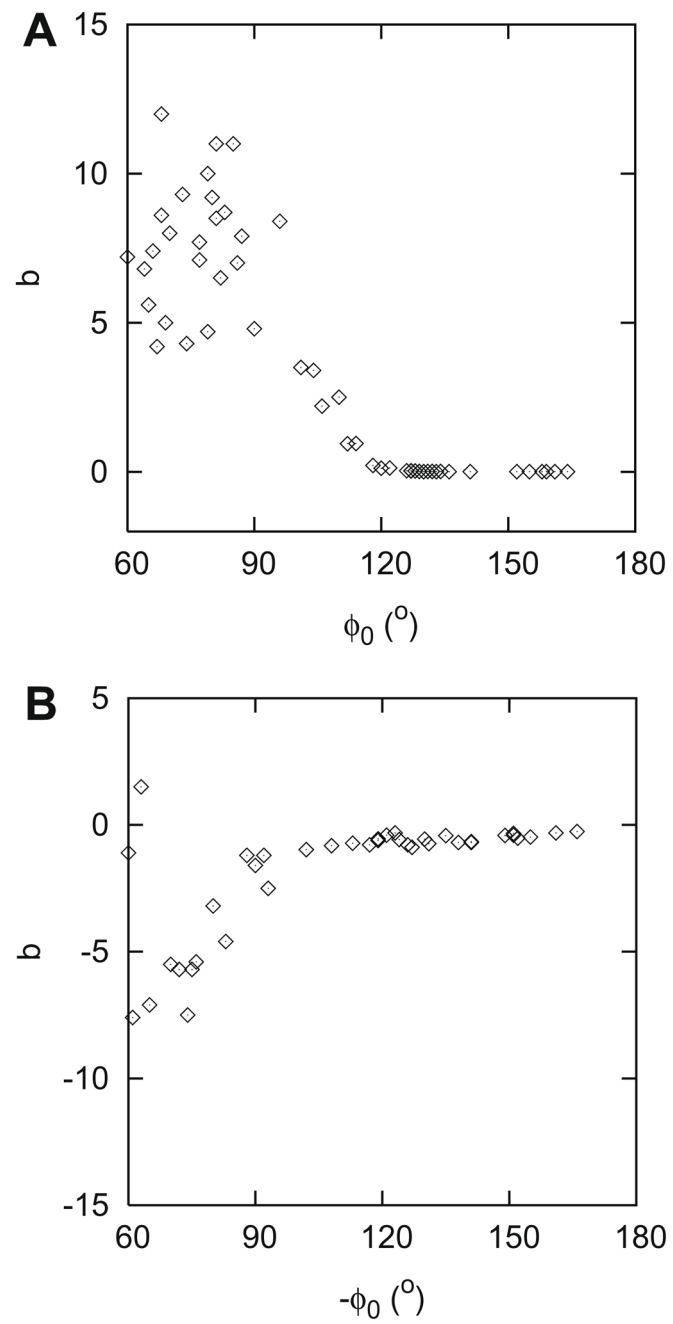


Fig. 4. Parameter b (as defined in Eq. (1)) – raw data – as a function of ϕ_0 for the superior (A) and the inferior (B) hemifield.

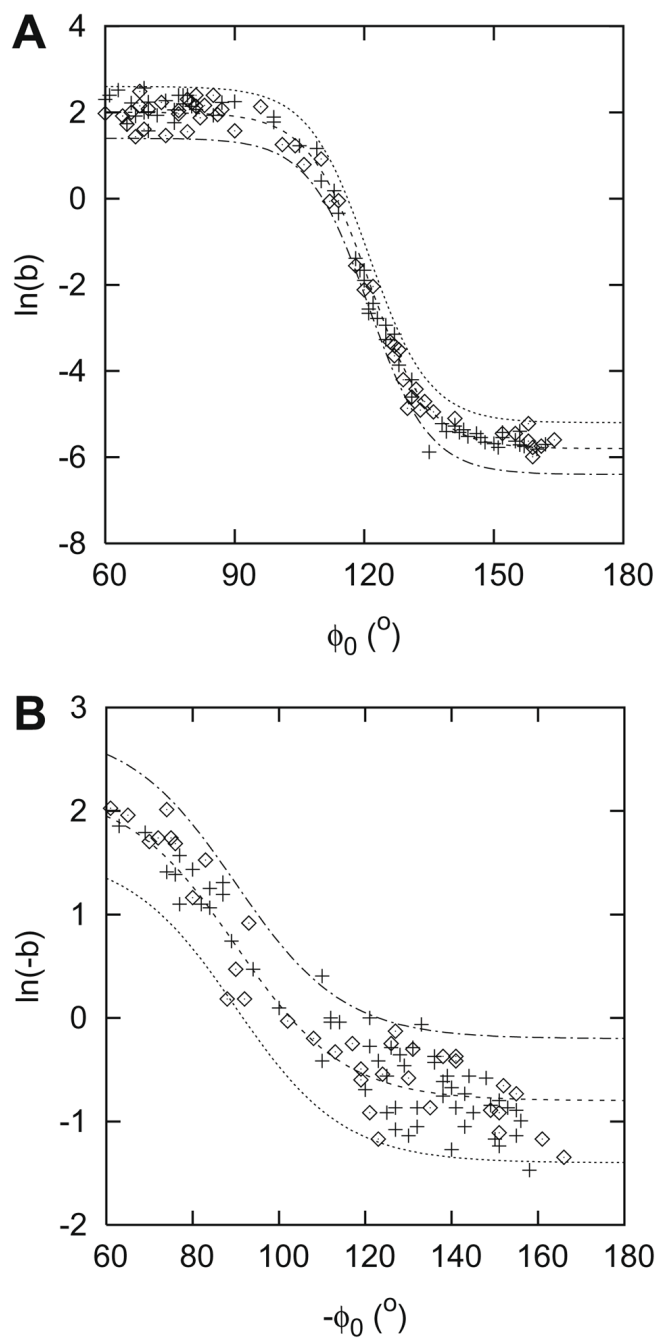


Fig. 5. Parameter b – fitted data – as a function of ϕ_0 for the superior (A) and the inferior (B) hemifield. Datapoints from both the original (diamond) and the independent (+) sample. The lines represent the average values and the 95% limits of the corresponding fits as described in Eqs. (5) and (6).

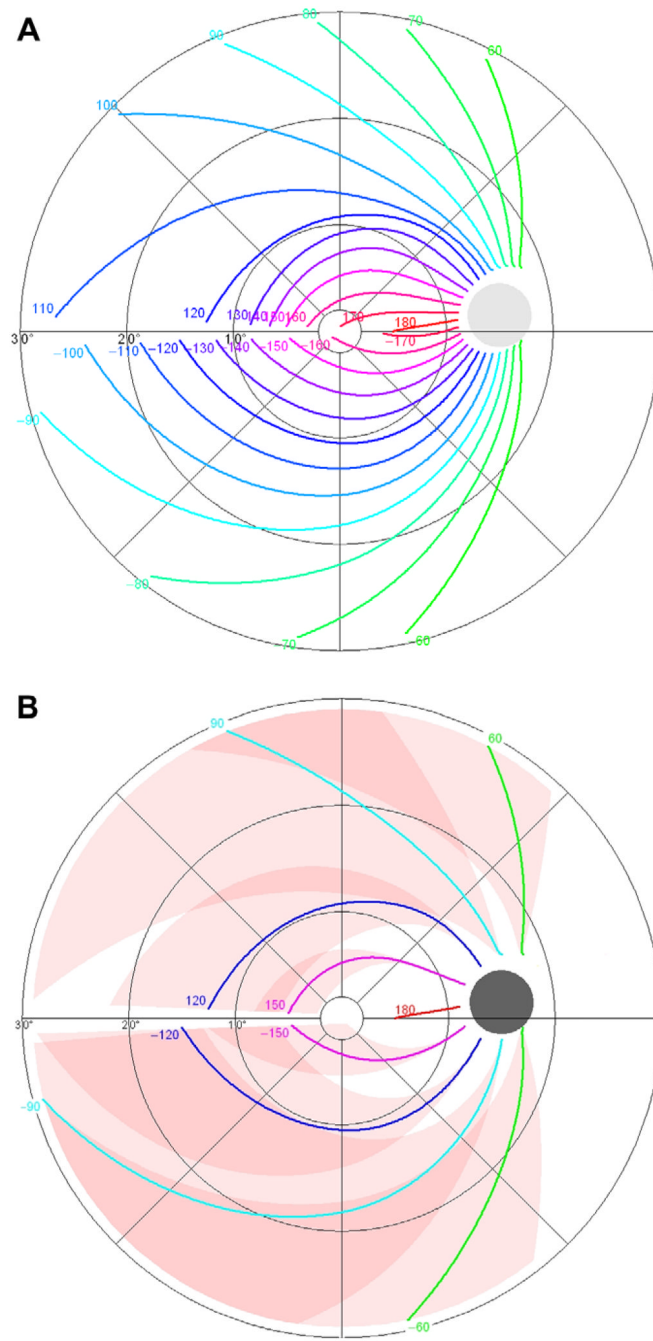


Fig. 6. Final model, average trajectories in 10° steps (A) and upper and lower limits of trajectories in 30° steps (B).

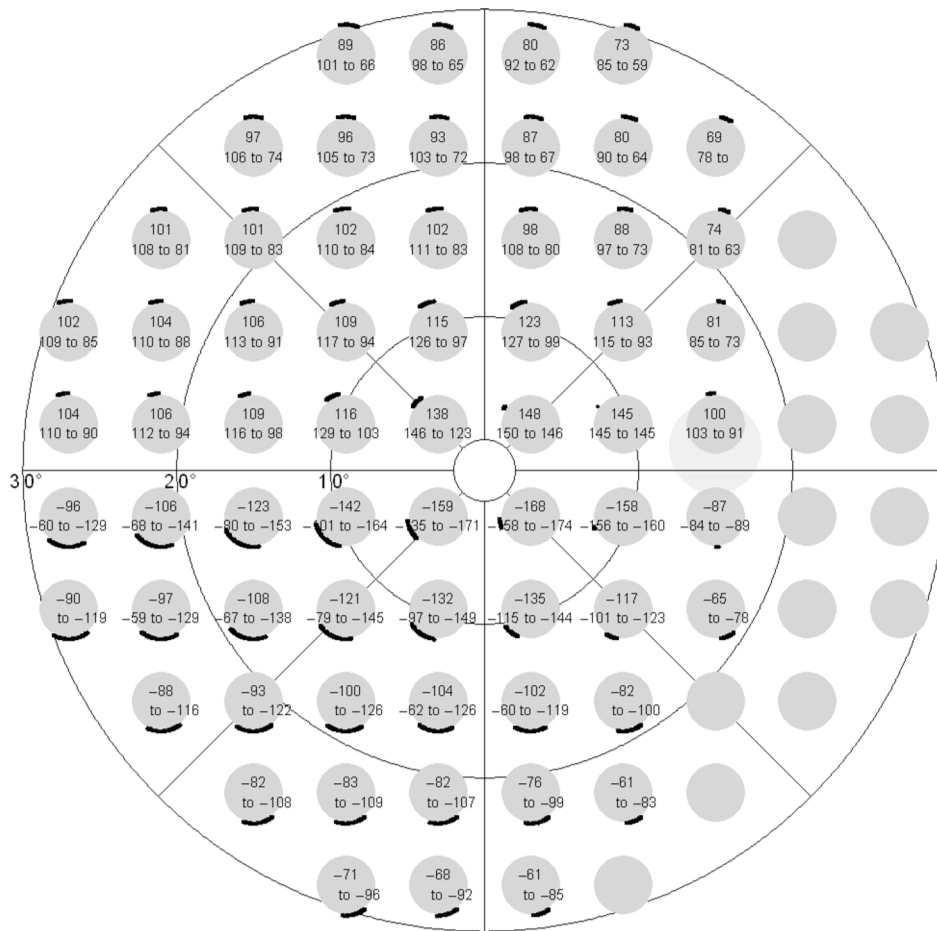


Fig. 7. Final model, reciprocal representation, with points from the 30–2 6° × 6° grid of the Humphrey Field Analyzer connected to the corresponding parts of the optic nerve head. The optic nerve head is presented upright; the visual field grid as projected on the retina, *i.e.*, mirrored along the *x*-axis.

Table 1

Inclusion criteria for fiber recordings.

Onset distance from (0,0)	$r_{min} \leq 5^\circ$
<i>Minimum length of a fiber</i>	
$0 \leq \varphi_0 \leq 60^\circ$	$r_{max} > 10^\circ$
$60 < \varphi_0 \leq 90^\circ$	$r_{max} > 15^\circ$
$90 < \varphi_0 \leq 150^\circ$	$r_{max} > 20^\circ$
$150 < \varphi_0 \leq 180^\circ$	$r_{max} > 15^\circ$
Number of datapoints per fiber	$n \geq 6$

r_{min} = onset of the fiber measured from the center of the optic disk; r_{max} = length of the fiber measured from the center of the optic disk; n = number of sampled datapoints.